PAPER

Check for updates

Enhanced extraction of organophosphorus pesticides from fruit juices using magnetic effervescent tablets composed of the NiFe$_2$O$_4$@SiO$_2$@PANI-IL nanocomposites†

Dechao Chen, Sai Ma, Xiaofan Zhang, Xuedong Wang, Ming Gao, Jieyi Li*
and Huili Wang [ID] *

The reported ionic liquid (IL)-based magnetic effervescent tablets are a result of direct addition of ILs and magnetic nanoparticles (MNPs). In effervescent reaction-enhanced microextraction procedures, the dissociation between ILs and MNPs easily leads to loss of ILs due to aqueous solubility, thereby decreasing the extraction efficiency. Herein, we attached a hydrophilic IL ([BMIM]Br) onto the surface of NiFe$_2$O$_4$@SiO$_2$@polyaniline (NiFe$_2$O$_4$@SiO$_2$@PANI-IL) to prepare novel core−shell-like multi-layer nanocomposites. Magnetic effervescent tablets were composed of Na$_2$CO$_3$ as an alkaline source, tartaric acid as an acidic source and as-synthesized nanocomposites as an extractant. The nanocomposites were used in an effervescent reaction-enhanced magnetic solid-phase extraction (ERMSE) for the extraction of four organophosphorus pesticides (OPPs) in fruit juices prior to HPLC-DAD detection. Under optimized conditions, this method provided low limits of detection (0.06−0.17 µg L^{-1}), high recoveries (80.6−97.3%) and excellent precision (1.1−5.2%) for OPP quantification in five fruit juices. Notably, the three-layer core−shell nanocomposites were efficiently recycled for at least eight extraction cycles with a recovery loss of <10%. The novelty of this study lies in: (1) for the first time, the ILs-based hybrid magnetic nanocomposites were prepared with appropriate pore size/volume and more active sites for OPPs; (2) the combination of the nanocomposites with effervescent tablets realizes rapid dispersion of CO$_2$ bubbles, and convenient magnetic separation/collection into one synchronous step; and (3) due to there being no requirement of electrical power, it is feasible for use in field conditions. Thus, the ERMSE method has excellent potential for conventional monitoring of trace-level OPPs in complex fruit juice matrices.

1. Introduction

Organophosphorus pesticides (OPPs) play an important role in controlling agricultural insects; however, their high toxicity has raised great public concern, especially in various foods.[1] The residues of OPPs in fruit juices constitute a serious risk to human health.[2] The Chinese government set the maximum residue limits of 10–50 µg kg^{-1} for OPPs in fruits and their related products (GB2763-2016, China Food and Drug Administration).[3] To ensure safety of fruit juices for human consumption, sensitive, rapid and robust analytical methodologies are required for OPP detection in fruit juices.

Compared to traditional methods, magnetic solid-phase extraction (MSPE) overcomes several shortcomings, such as

use of large volumes of organic solvent, requirement for specialized devices and time-consuming processing.[4,5] Among magnetic adsorbents utilized for MSPE, magnetic nanoparticles (MNPs) are widely used in the adsorption of OPPs due to their excellent characteristics. Among them, NiFe$_2$O$_4$ has received wide attention because of its advantageous properties, such as high surface area and strong magnetic response.[6–8] However, due to the high chemical reactivity of bare NiFe$_2$O$_4$, it readily oxidizes in air leading to a loss of dispersibility and adsorption capacity. Hence, a protective layer is often applied to ensure chemical stability and enhance dispersibility.[9–11]

Silica is often selected as a coating layer for NiFe$_2$O$_4$ MNPs because of its chemical stability, biocompatibility and ease for surface modification.[9,10] For example, methyl blue was adsorbed from aqueous solution by magnetic 0.9NiFe$_2$O$_4$/0.1SiO$_2$ nanocomposites.[11] Some modification of nanocomposite surfaces by either functionalization or coating with other solid support or functional groups (*e.g.*, natural, conductive, and synthetic polymers) is required to enhance resolution and extraction

School of Environmental Science and Engineering, Suzhou University of Science and Technology, Suzhou 215009, China. E-mail: 100913915@qq.com; whuili@163.com; Fax: +86-512-68095950; Tel: +86-512-68095950

efficiency.[12] Among the conductive polymers, polyaniline (PANI) has attracted a great deal of attention due to its multifunctional properties (*e.g.*, hydrophobicity, acid–base character, π–π interactions and electrical activity), easy synthesis and permeable porous structure.[13,14] In the synthesis of PANI, it is possible to add amphiphilic compounds, called surfactants, which interact with each other to form molecular aggregates, called micelles, which form a porous media.[15] Consequently, PANI is applied in separation science, in areas such as packing material in MSPE and fiber material for SPME.[16] Especially, PANI has been modified with MNPs to extract various types of pollutants from environmental matrices, such as prepared Fe_3O_4@-SiO_2@polyaniline (PANI) MNPs to adsorb Se and Te,[17] PANI nanofiber synthesized on graphene oxide (PANI-GO) surfaces for extraction of Pb^{2+} in food samples[18] and restricted access macroporous magnetic polyaniline for coumarin detection in rat plasma.[15]

Ionic liquids (ILs) refer to a class of organic salts composed of various inorganic and organic anions and organic cations.[19,20] By changing the structure of ionic moieties or polymerization, the properties of ILs can be modified and optimized for different target analytes.[21] In recent years, ILs have been employed to increase the extraction efficiency by loading them onto the surface of polymers or MNPs,[22] which can interact with organic chemicals *via* electrostatic interactions, hydrogen bonding, π–π stacking and hydrophilic/hydrophobic interactions. Generally, the prominent benefits of using ILs as coating materials on MNPs are to improve the selectivity, sensitivity and extraction efficiency for target analytes.[23] Notably, the integration of ILs with PANI will supply more surface-active groups (*e.g.*, carboxyl, hydroxyl and ammonium groups), yielding stronger molecular interactions between PANI-IL and targeted chemicals.

Based on the above considerations, magnetic nanocomposites based on the combination of $NiFe_2O_4$@SiO_2, PANI and ILs were prepared, hereafter referred to as $NiFe_2O_4$@-SiO_2@PANI-IL. The MNPs were employed as an adsorbent in an effervescent reaction-enhanced microextraction for efficient extraction of OPPs in fruit juices. The $NiFe_2O_4$@SiO_2@PANI-IL nanocomposites demonstrated several advantages aimed at improving the dispersibility of nanocomposites and extraction efficiency, such as moderate specific surface area and pore size, an abundance of surface-active groups, rapid magnetic separation and reduced agglomeration of nanoparticles. Nowadays, effervescent reaction-enhanced microextraction is based on a simple reaction that generates CO_2 bubbles, which accelerates the dispersion of MNPs in solution.[24,25] The process of magnetic effervescent tablet-assisted dispersive extraction can eliminate the use of dispersive solvents in microextraction, realize rapid magnetic separation, avoid centrifugation/stirring steps and save processing time.

The aim of this work was to develop a novel magnetic nanocomposite based on IL-coated $NiFe_2O_4$@SiO_2@PANI hybrid MNPs. Subsequently, the hybrid nanocomposites were employed in an effervescent reaction-enhanced magnetic solid-phase extraction (ERMSE) for preconcentration/extraction of four common OPPs from fruit juice samples prior to detection by liquid chromatography. Under optimized conditions, the

ERMSE methodology demonstrated efficient adsorption/ extraction of trace-level OPPs, thereby showing excellent potential for routine monitoring of OPPs in fruit juices.

2. Experimental

2.1. Reagents and materials

Analytical standards for four OPPs (methamidophos, malathion, parathion, diazinon) with 99% purity, and analytical-grade $FeCl_3 \cdot 6H_2O$ and $Ni(NO_3)_2 \cdot 6H_2O$ were purchased from Zhongke Quality Inspection Biotechnology (Beijing, China). Chromatographic-grade methanol, acetonitrile, ethanol, acetone and ethyl acetate were obtained from Aladdin (Shanghai, China). A series of analytical-grade chemicals were acquired from Tansoole (Shanghai, China): sodium hydroxide (NaOH), sodium carbonate (Na_2CO_3), hydrochloride acid (HCl), polyethylene glycol (PEG), tartaric acid (TTA), tetraethoxysilane (TEOS), aniline, ammonium persulfate (APS) and the ionic liquid, 1-butyl-3-methylimidazolium bromide ([BMIM]Br). Each OPP standard was dissolved in methanol to prepare a stock solution (100 mg L^{-1}) and stored at 4 °C. Ultrapure water (>18.2 MΩ-cm, Millipore, Billerica, MA, USA) was used throughout this study. The 0.22 μm nylon (NL) and 0.45 μm polyether sulfone (PES) membrane filters were purchased from Anpel Scientific Instrument (Shanghai, China).

2.2. Instrumentation

Quantification of OPPs was performed on a Shimadzu HPLC-DAD (LC-20AT). A Zorbax Eclipse XDB-C_{18} column (5 μm, 150 mm × 4.6 mm) was used for separating the analytes. HPLC-DAD operational conditions were as follows: flow rate, 0.9 mL min^{-1}; column temperature, 30 °C; mobile phase, methanol–water at 65%:35% v/v; detection wavelength, 270 nm and injection volume, 20 μL. The structure and morphology of nanomaterials were characterized by scanning electron microscopy (SEM, Sigma300, Germany) and transmission electron microscopy (TEM, JEM2010, USA). Fourier-transform infrared (FT-IR) spectra were recorded on a Nicolet IS50 spectrometer with a range of 400–4000 cm^{-1}. Powder X-ray diffraction (XRD) of nanomaterials was obtained by an EDX-720 X-ray power diffractometer (Agilent, USA) with a Cu Kα source (1.54056 Å) at room temperature between 5° and 90° 2θ. Brunauer–Emmett–Teller (BET) surface area was measured by N_2 adsorption–desorption at 77 K using an ASAP 2020 system (Quantachrome, USA). Magnetic properties were investigated using a vibrating sample magnetometer (VSM, San Diego, CA, USA) with an applied field between −20 000 Oe and 20 000 Oe at room temperature. Zeta potential was measured using a zeta potential analyzer (Malvern, UK). Thermogravimetric analysis (TGA) was determined at a heating rate of 10 °C min^{-1} over a temperature range of 50 to 700 °C under nitrogen flow (SDT Q600 Thermal Analyzer, Perkin Elmer, Waltham, MA, USA).

2.3. Synthesis of $NiFe_2O_4$@SiO_2@PANI-IL nanocomposites

2.3.1. $NiFe_2O_4$ MNPs. Magnetite $NiFe_2O_4$ nanoparticles were prepared by using a hydrothermal method.[24] First,

FeCl$_3 \cdot$6H$_2$O (5.4 g) and Ni(NO$_3$)$_2 \cdot$6H$_2$O (2.9 g) were dissolved in 100 mL ultrapure water. After 10 min ultrasound, 0.11 g of PEG was added and further sonicated for 5 min.[26] Then, the pH of the resulting solution was adjusted to 7.0 using 0.9 mol L^{-1} NaOH. Next, the mixture was transferred to a 100 mL Teflon-lined stainless autoclave and heated at 160 °C for 12 h followed by cooling to room temperature. Finally, the precipitates were collected using a magnet and washed for three cycles with ultrapure water and ethanol, before drying in a vacuum oven at 60 °C for 6 h.

2.3.2. NiFe$_2$O$_4$@SiO$_2$ nanomaterials. NiFe$_2$O$_4$ MNPs (3.0 g) were dispersed in 25 mL of ethanol and ultrasonicated for 10 min. The solution was stirred at ambient conditions under a N$_2$ flow with the pH adjusted to 11 (15%, NH$_3 \cdot$H$_2$O). Next, 2 mL of TEOS was added to the solution and continuously stirred for 1 h. Subsequently, NiFe$_2$O$_4$@SiO$_2$ nanomaterials were magnetically separated and washed for 3 cycles with ultrapure water and ethanol, followed by drying in a vacuum oven for 3 h at 60 °C.

2.3.3. NiFe$_2$O$_4$@SiO$_2$@PANI-IL nanocomposites. First, 1.5 g of ammonium persulfate (APS) and 1.0 g of aniline were dissolved in 40 mL of 0.25 M HCl. The mixture was then stirred for 2 h and stored at 4 °C. Next, the aforementioned mixture was added dropwise to 60 mL ethanol containing 1.5 g of NiFe$_2$O$_4$@SiO$_2$ and 1.0 g of [BMIM]Br. After 12 h of stirring, the synthesized NiFe$_2$O$_4$@SiO$_2$@PANI-IL nanocomposites were rinsed for 3 cycles with ethanol and water, before drying in a vacuum oven at 60 °C. Finally, the dried nanomaterial was ground into a powder and sealed for further use (Fig. 1A).

2.4. Preparation of the magnetic effervescent tablets

Initially, Na$_2$CO$_3$ and TTA were dried in an oven for 1 h at 60 °C and stored in a desiccator before use. Then, a mixture of Na$_2$CO$_3$ (212 mg) and TTA (300 mg), and 15 mg of prepared NiFe$_2$O$_4$@SiO$_2$@PANI-IL nanocomposites were mixed and manually blended in an agate mortar. After grinding, the power was compressed into a magnetic effervescent tablet (8 mm

diameter × 2.5 mm thickness) by a 5T/8MM 5T Punch Press (Shanghai, China). The as-pressed effervescent tablets were stored in a desiccator at room temperature prior to use (Fig. 1B).

2.5. Fruit juice sample preparation

Five types of fruit juice samples (apple, pear, orange, peach and mango) were provided by Jialefu Supermarket (Suzhou, China). Aliquots (30 mL) of the fresh juice samples were centrifuged at 5000 rpm for 10 min and the supernatants filtered through a 0.45 μm membrane filter. Finally, the filtrate was diluted 1 : 2 using Milli-Q ultrapure water for use in the following ERMSE procedures.

2.6. ERMSE procedures

A schematic illustration of the ERMSE method is depicted in Fig. 1C. First, an aliquot (8 mL) of the pretreated juice was introduced into a 15 mL conical centrifuge tube. Next, a magnetic effervescent tablet was placed into the tube where it produced a vigorous reaction of bubbles (CO$_2$) throughout the reaction vessel. The effervescent tablet remained active for ~3–4 min, resulting in homogeneous dispersion of the nanocomposites throughout the aqueous solution. Then, the nanocomposite adsorbent enriched with the analytes was collected by placing an external magnet alongside the centrifuge tube. The supernatant was carefully discarded by pipette, and an appropriate volume of elution solvent added to elute the OPPs from the nanocomposites. The collected eluate was filtered using a 0.45 μm filter, and redissolved in 100 μL methanol after being dried with a gentle nitrogen gas flow. Finally, 20 μL of the resulting solution was subjected to HPLC/DAD detection.

3. Result and discussion

3.1. Characterization of NiFe$_2$O$_4$@SiO$_2$@PANI-IL MNPs

3.1.1. SEM and TEM analyses of coated nanocomposites. Morphologies of the NiFe$_2$O$_4$, NiFe$_2$O$_4$@SiO$_2$ and
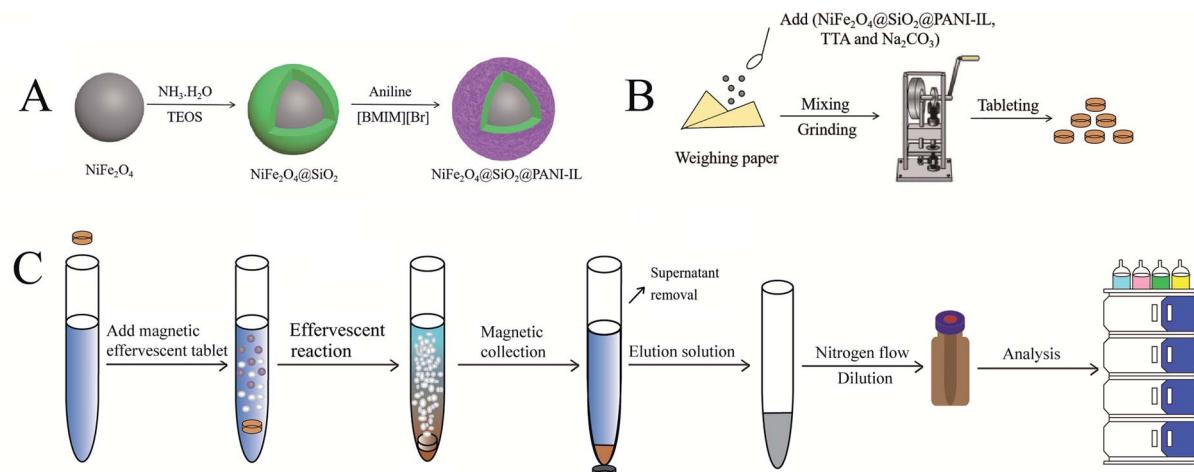
**Fig. 1** Schematic representation of the ERMSE procedures. Note: (A) synthesis of the NiFe$_2$O$_4$@SiO$_2$@PANI-IL nanocomposites; (B) preparation of effervescent tablets; (C), operational procedures for the ERMSE method.

$NiFe_2O_4$@SiO_2@PANI-IL were examined by SEM and TEM (Fig. 2). $NiFe_2O_4$ nanoparticles exhibited an obvious agglomeration phenomenon (Fig. 2A and D). The SiO_2 attached on the $NiFe_2O_4$ surface protected the MNPs from being corroded and oxidized in the air, and further agglomerated in the aqueous phase. $NiFe_2O_4$@SiO_2 showed sphere-shaped nanoparticles with increased particle size as compared to $NiFe_2O_4$ nanoparticles (Fig. 2B and E). Compared to the pure $NiFe_2O_4$ MNPs, SEM images of $NiFe_2O_4$@SiO_2@PANI-IL displayed a multi-layer sphere, but their surface became rough (Fig. 2C). TEM observations showed smaller nanoparticles attached onto the surface of the $NiFe_2O_4$ core as PANI coated the surface of the SiO_2 layer, and PANI acted as a bridge to load ILs (Fig. 2F). Introduction of ILs onto the surface of the core–shell structure led to more surface active sites on the MNPs, contributing to potentially higher extraction efficiency for OPPs.

3.1.2. EDS elemental mapping.

Elemental analysis by EDS mapping demonstrated the presence of O, Fe, Ni, Si, C and N in the synthesized nanocomposites (Fig. 3); atomic percentages are reported in ESI Table 1.† As for $NiFe_2O_4$@SiO_2@PANI-IL nanocomposites, the elemental percentages for O, Fe, Ni, Si, C and N were 16.6, 2.5, 1.2, 3.4, 65.6 and 6.7%, respectively. Compared to $NiFe_2O_4$ and $NiFe_2O_4$@SiO_2 nanoparticles, the $NiFe_2O_4$@SiO_2@PANI-IL surface had lower O, Fe, Ni and Si contents, but higher C and N concentrations indicating successful synthesis of magnetic core–shell nanocomposites. EDS mapping of $NiFe_2O_4$@SiO_2@PANI-IL identified the presence of Fe (from $NiFe_2O_4$), Ni (from $NiFe_2O_4$), O (from $NiFe_2O_4$@SiO_2), N (from PANI and [BMIM]Br), and C (from PANI and [BMIM]Br). These results confirm the uniform distribution of multi-layer coatings (SiO_2, PANI and [BMIM]Br) over the surface of the $NiFe_2O_4$ nanoparticles, and also the successful synthesis of the core–shell structure of $NiFe_2O_4$@SiO_2@PANI-IL nanocomposites.

3.1.3. FT-IR characterization.

FT-IR spectra for $NiFe_2O_4$, $NiFe_2O_4$@SiO_2 and $NiFe_2O_4$@SiO_2@PANI-IL MNPs are
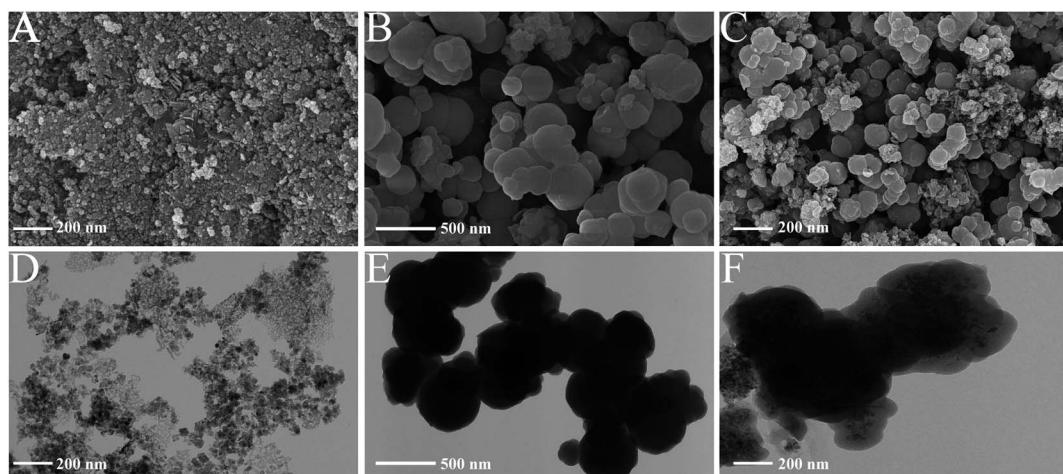
Fig. 2 SEM images of $NiFe_2O_4$ (A), $NiFe_2O_4$@SiO_2 (B) and $NiFe_2O_4$@SiO_2@PANI-IL (C); TEM images of $NiFe_2O_4$ (D), $NiFe_2O_4$@SiO_2 (E) and $NiFe_2O_4$@SiO_2@PANI-IL (F).
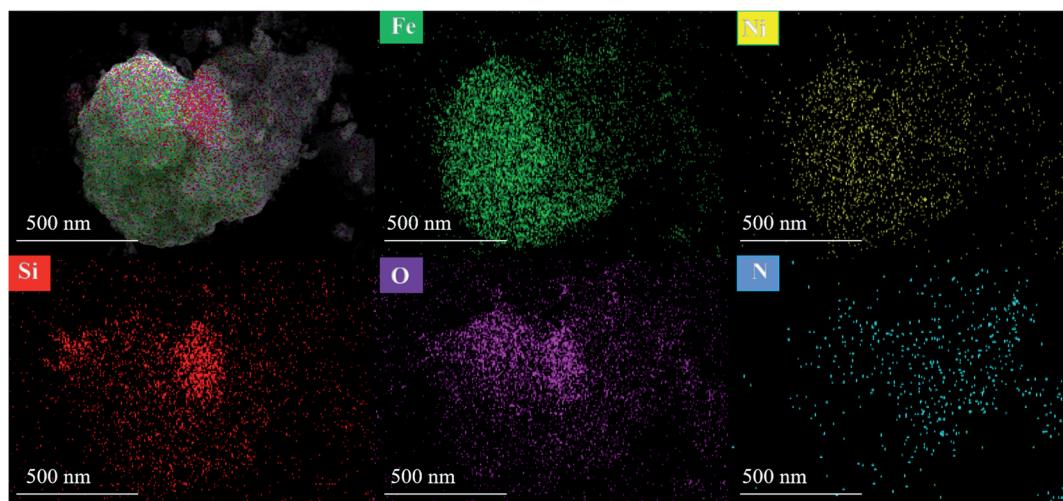

Fig. 3 EDS mapping of the $NiFe_2O_4$@SiO_2@PANI-IL nanocomposites.

displayed in Fig. 4A. $NiFe_2O_4$ MNPs displayed absorption bands at 454, 600, 1342, 1628 and 3419 cm^{-1} corresponding to the stretching vibration peaks for Ni–O, Fe–O, C=O, N–O and O–H, respectively. Compared to the $NiFe_2O_4$ spectrum, new peaks around 700–1000 and 1100 cm^{-1} appeared in both $NiFe_2O_4$@-SiO_2 and $NiFe_2O_4$@SiO_2@PANI-IL nanocomposites, which were attributed to the C–H stretching vibration and Si–O–Si lattice vibration of SiO_2, respectively. These results indicate that SiO_2 was successfully encapsulated on the surface of the $NiFe_2O_4$ MNPs by physical and chemical adsorption. The peaks at 1299 and 1487 cm^{-1} were related to the C=O and C=C groups of PANI-IL. The typical stretching vibration peak of C=N at 1233 cm^{-1}, resulting from PANI and [BMIM]Br, indicated that the PANI-IL was successfully attached onto the surface of $NiFe_2O_4$@SiO_2. Hence, FT-IR analysis verified the successful preparation of the $NiFe_2O_4$@SiO_2@PANI-IL nanocomposites.

3.1.4. XRD characterization. The crystalline structures of $NiFe_2O_4$, $NiFe_2O_4$@SiO_2 and $NiFe_2O_4$@SiO_2@PANI-IL were confirmed by XRD (Fig. 4B). The main peaks at 2θ values of 18.3, 30.4, 44.2, 54.7, 57.1 and 63.5° were assigned to the (111), (220), (400), (422), (511) and (440) reflections of $NiFe_2O_4$ (PDF#74-2081 standard pattern), respectively. Compared to $NiFe_2O_4$, the peak for $NiFe_2O_4$@SiO_2 around 24.6° was assigned to the (002) plane of SiO_2.[27] There were no prominent differences in XRD profiles between $NiFe_2O_4$@SiO_2 and $NiFe_2O_4$@SiO_2@PANI-IL, implying that the PANI-IL coating did not affect the crystal structure of $NiFe_2O_4$@SiO_2 MNPs. Results of XRD characterization provided further evidence for successful synthesis of the nanocomposites.

3.1.5. Magnetic properties. Saturated magnetization values for $NiFe_2O_4$, $NiFe_2O_4$@SiO_2 and $NiFe_2O_4$@SiO_2@PANI-IL MNPs were 36.2, 29.5 and 23.9 emu g^{-1}, respectively (Fig. 4C). Higher magnetic saturation values reflect stronger magnetic properties. Although the saturation magnetization values of the nanocomposites were reduced by surface coatings, rapid separation from aqueous solution was still achieved due to the relatively
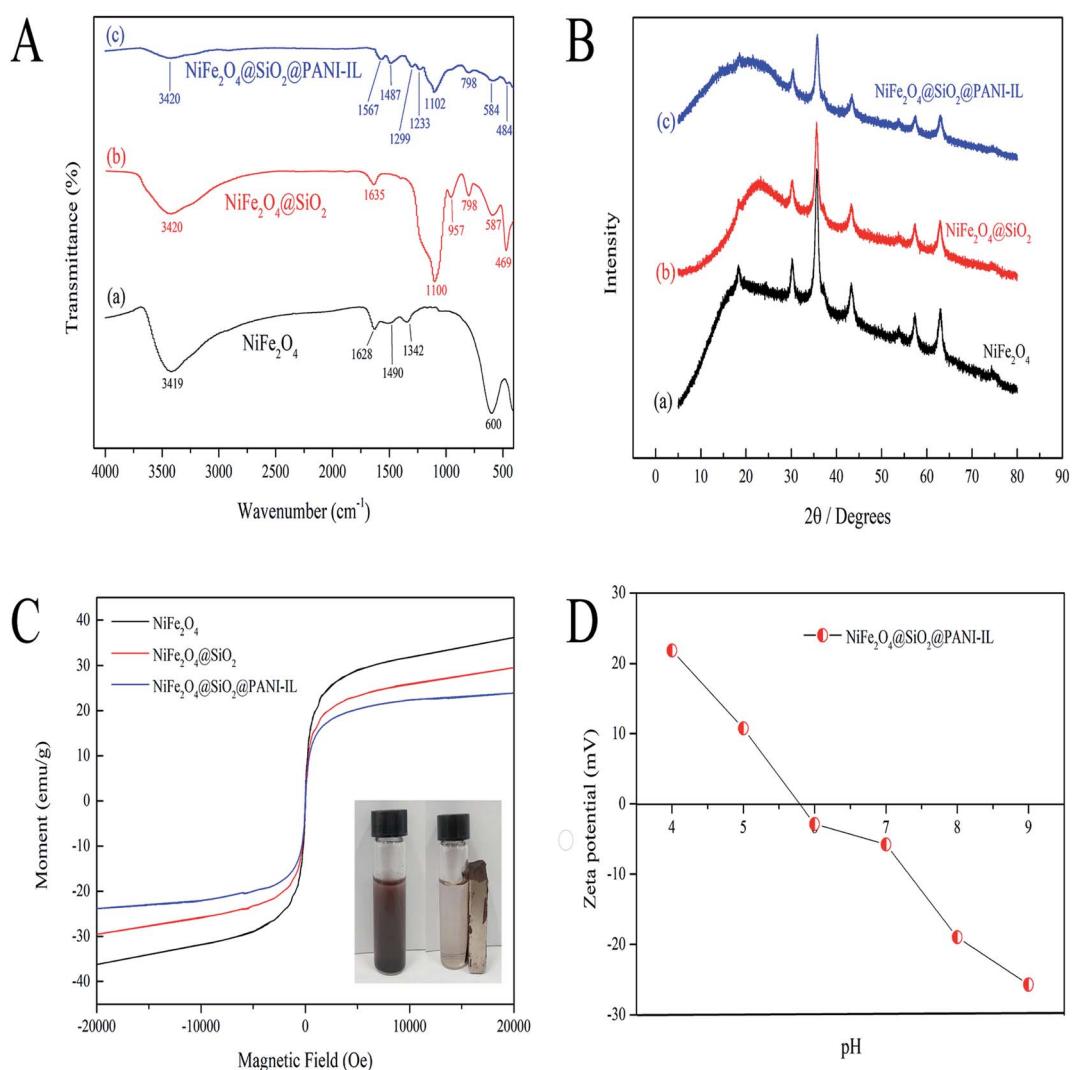

Fig. 4 FT-IR spectrum of $NiFe_2O_4$ (A-a), $NiFe_2O_4$@SiO_2 (A-b) and $NiFe_2O_4$@SiO_2@PANI-IL (A-c); XRD patterns of $NiFe_2O_4$ (B-a), $NiFe_2O_4$@SiO_2 (B-b) and $NiFe_2O_4$@SiO_2@PANI-IL (B-c); Magnetic properties of nanocomposites (C); zeta potentials of nanocomposites at different pH values (D).

high saturation magnetization of NiFe$_2$O$_4$@SiO$_2$@PANI-IL (Inset of Fig. 3C).

3.1.6. Zeta potential characterization. The point of zero charge (PZC) is an important variable for assessing the surface charge characteristics of nanocomposites. The PZC of NiFe$_2$O$_4$@SiO$_2$@PANI-IL nanocomposites was pH = 5.8, indicating that the net surface charge of the nanocomposites was positive at pH < 5.8, but negative at pH > 5.8 (Fig. 4D). At a near-neutral charge state (pH = 5.8), the nanomaterials should possess their highest extraction efficiency for the molecular-state OPPs.

3.1.7. N$_2$ adsorption–desorption isotherms. The BET surface area along with pore volume and size were measured for NiFe$_2$O$_4$, NiFe$_2$O$_4$@SiO$_2$ and NiFe$_2$O$_4$@SiO$_2$@PANI-IL using N$_2$ adsorption–desorption dynamics. BET surface areas of NiFe$_2$O$_4$, NiFe$_2$O$_4$@SiO$_2$ and NiFe$_2$O$_4$@SiO$_2$@PANI-IL were 104.5, 173.1 and 81.1 m^2 g^{-1}, respectively (Fig. 5; ESI Table 2†). Compared to NiFe$_2$O$_4$ and NiFe$_2$O$_4$@SiO$_2$, the decreased surface area of NiFe$_2$O$_4$@SiO$_2$@PANI-IL nanocomposites appears to result from the introduction of multiple surface functional groups, accompanying with partial agglomeration of the MNPs.[28] Relative to the NiFe$_2$O$_4$ (0.302 cm^3 g^{-1}), the decreased pore volume of NiFe$_2$O$_4$@SiO$_2$ (0.059 cm^3 g^{-1}) was likely due to the encapsulation of SiO$_2$ nanoparticles into NiFe$_2$O$_4$. However, compared to the NiFe$_2$O$_4$@SiO$_2$, the higher pore volume of NiFe$_2$O$_4$@SiO$_2$@PANI-IL (0.136 cm^3 g^{-1}, Fig. 5C) may result from generation of mesoporous structures between the interconnected nanofibers in PANI-IL, providing more active paths and sites for adsorption. Mean pore size of NiFe$_2$O$_4$,

NiFe$_2$O$_4$@SiO$_2$ and NiFe$_2$O$_4$@SiO$_2$@PANI-IL was 13.7, 14.1 and 17.9 nm, which were all in the mesoporous size range (2–50 nm). Generally, the moderate surface area and mesoporous structure provide abundant sites for sorption of pollutants, rendering NiFe$_2$O$_4$@SiO$_2$@PANI-IL an effective adsorbent for OPPs.

3.1.8. Thermogravimetric properties. Thermal stability of the three MNPs was assessed by TGA in the temperature range of 50–700 °C under nitrogen flow. Mass loss below 200 °C was in the range of 5–9%, which was ascribed to evaporation of sorbed water (Fig. 5D). In the temperature range of 200–450 °C, mass loss of NiFe$_2$O$_4$@SiO$_2$@PANI-IL nanocomposites was about 20%, which may represent loss of unbound HCl.[29] A further mass loss of 30% at temperatures between 450–575 °C was attributed to pyrolysis of the PANI chains. In sharp contrast, the TGA curve of NiFe$_2$O$_4$ showed a mass loss of ~8% over the 30–700 °C temperature range assigned to the loss of physically and chemically bound water molecules (Fig. 5D). The similar low-level mass loss for NiFe$_2$O$_4$@SiO$_2$ and NiFe$_2$O$_4$ verifies the good thermal stability of MNPs in the core–shell microspheres.

3.2. Optimization of ERMSE operational parameters

3.2.1. Composition of acidic and basic salts for effervescent tablet. Effervescent tablets (mixture of effervescent precursors) play an important role in the ERMSE procedures by acting as a vigorous dispersant. Effervescent tablets are composed of three main components: acidic salt, alkaline salt
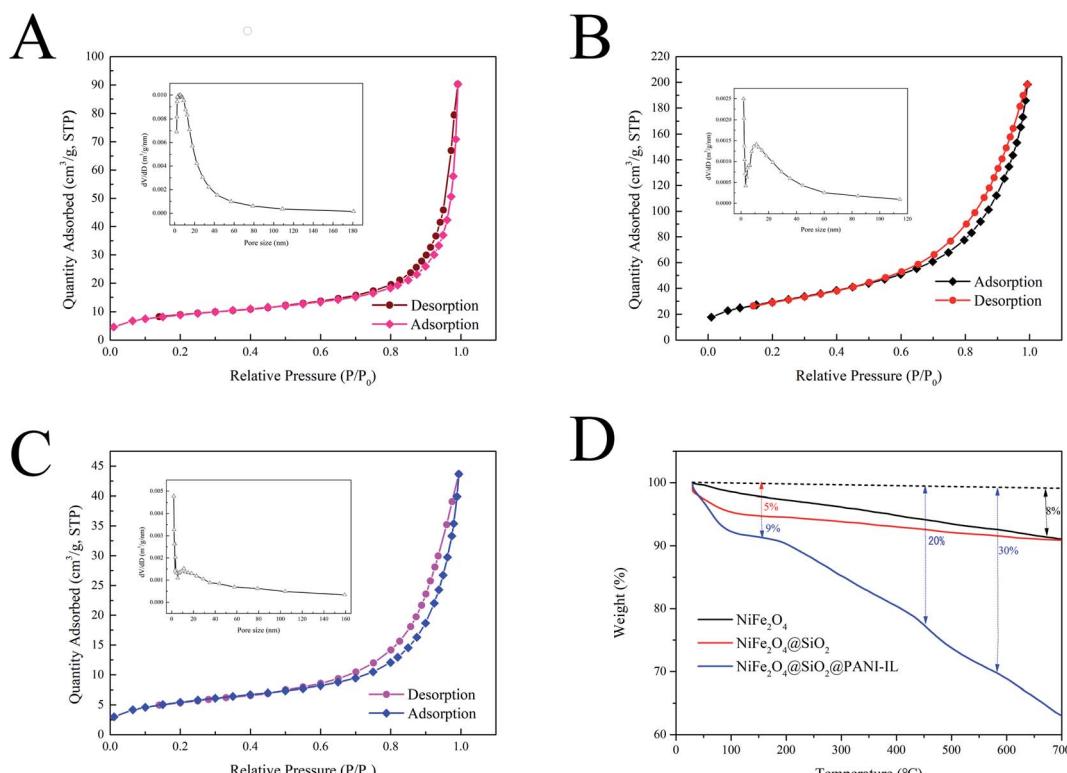

Fig. 5 Nitrogen adsorption–desorption isotherms for NiFe$_2$O$_4$ (A), NiFe$_2$O$_4$@SiO$_2$ (B) and NiFe$_2$O$_4$@SiO$_2$@PANI-IL nanocomposites (C); TGA profiles of the different nanocomposite coatings (D).

and extractant/adsorbent.[23] According to previous reports,[30,31] we tested two conventional acidic salts and two alkaline salts as potential tablet components, Na_2CO_3 and $NaHCO_3$ as alkaline salts and NaH_2PO_4 and tartaric acid (TTA) as acidic salts. We assessed four different tablet combinations: Na_2CO_3 + NaH_2PO_4, $NaHCO_3$ + NaH_2PO_4, Na_2CO_3 + TTA, and $2NaHCO_3$ + TTA. The Na_2CO_3 + TTA combination provided the highest overall mean extraction recoveries (ERs) for the four OPPs. With respect to individual OPP ERs, Na_2CO_3 + TTA had the highest ERs for methamidophos, malathion and parathion, while Na_2CO_3 + NaH_2PO_4 had the highest ER for diazinon (Fig. 6A). The Na_2CO_3 + TTA tablet, composed of 212 mg of Na_2CO_3, 300 mg of $C_4H_6O_6$ and 15 mg nanocomposites, produced a vigorous effervescence intensity and reaction time (~4 min), consistent with previous results obtained by Ding et al.[30] and Wu et al.[31] Given its superior performance, the Na_2CO_3+ TTA tablet was selected as the acidic/alkaline source in preparation of magnetic effervescent tablets.

3.2.2. Amount of $NiFe_2O_4@SiO_2@PANI$-IL nanocomposites as adsorbent. Magnetic nanocomposites enhance the adsorption/extraction of OPPs from complex matrices due to their high specific surface area, appropriate PZC yielding suitable surface charge characteristics, abundant surface adsorption groups and efficient collection from solution by a strong magnetic field.[3] The effects of the amount of MNPs on the ERs were investigated over the range of 5–30 mg. The ERs for all four
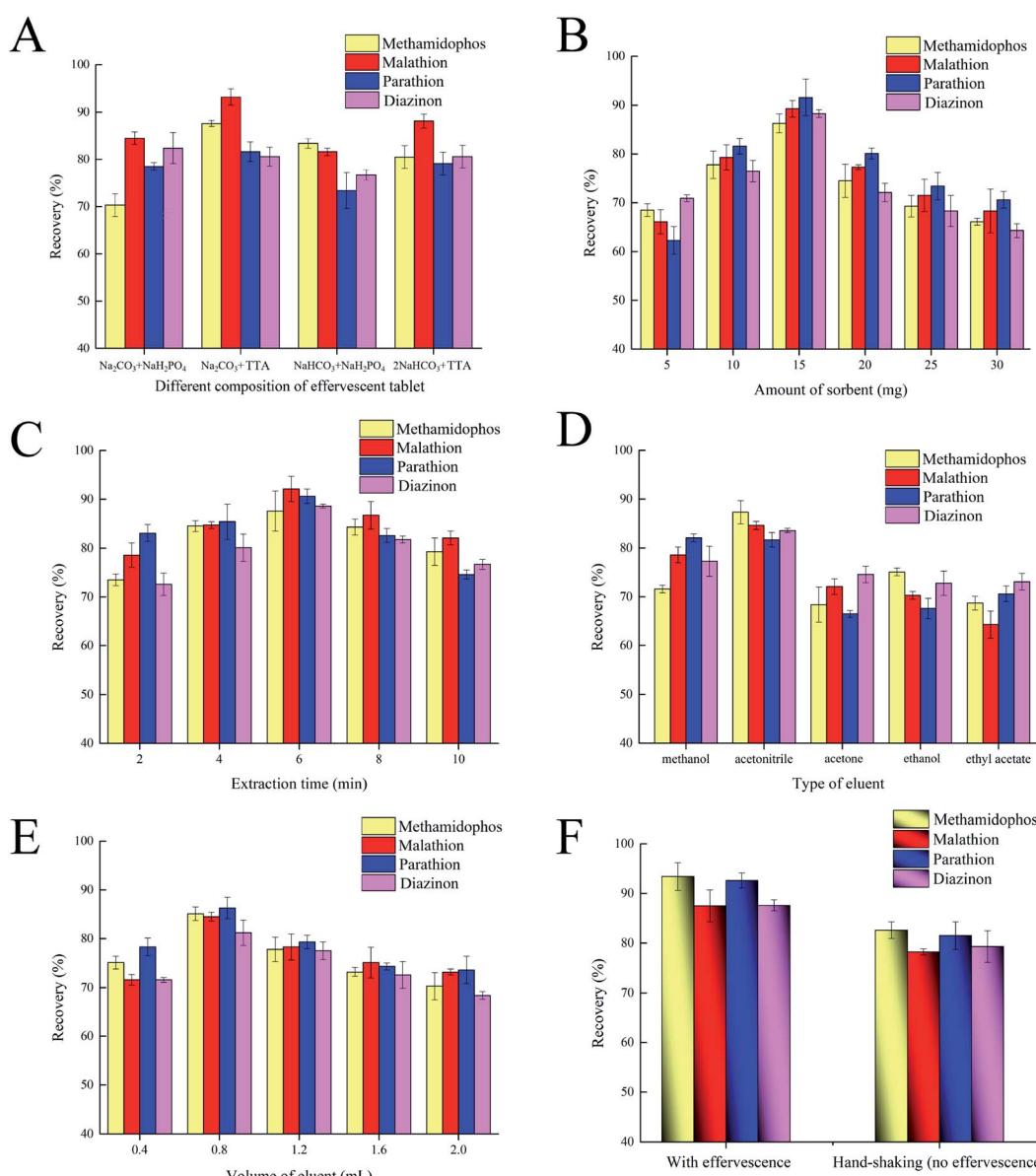
Fig. 6 Effects of experimental variables on the ERs for OPPs. Note: (1) (A), effects of different composition of effervescent tablets on ERs; (B), amount of the nanocomposites; (C), extraction time; (D), type of elution solvent; (E) volume of elution solvent; (F) comparison of ERs with effervescent reaction versus 4 min hand-shaking (no effervescence); (2) error bar indicates the standard deviation ($n = 3$); (3) spiked level of each OPP species at 20 µg L^{-1}.

OPPs increased with increasing adsorbent doses from 5 to 15 mg, but decreased with further increases from 20 to 30 mg (Fig. 6B). As a consequence, 15 mg was chosen as the optimum quantity of adsorbent for the extraction process.

3.2.3. Extraction time. Extraction time indicates the interval from dispersion to separation of the nanocomposites and is an important parameter for optimizing the ERs for OPPs in the ERMSE procedures. An appropriate extraction time leads to improvements in adsorption by MNPs, purification effects and extraction efficiency.[32] The effect of extraction time was examined in the range of 2–10 min (Fig. 6C). The ERs for the four OPPs increased gradually with increasing extraction time from 2 to 6 min, followed by a decrease from 6 to 10 min. Accordingly, 6 min was adopted as the optimum extraction time for subsequent experiments.

3.2.4. Type and volume of elution solvent. The elution solvent has a significant effect on the ERs for OPPs due to differential polarities. Five common eluent solvents (methanol, acetonitrile, acetone, ethanol and ethyl acetate) were compared for their elution efficiency. Acetonitrile gave the highest average ERs for the four OPPs ($\sim$85%), which was much higher than for methanol ($\sim$75%) (Fig. 6D). Acetone, ethanol and ethyl acetate produced relatively lower ERs ($\sim$65%) for the four OPPs. Thus, acetonitrile was selected as the optimal solvent in further optimization studies.

Elution solvent volume was examined over the range of 0.4 to 2.0 mL for ERs of the four OPPs. The ERs increased from 0.4 to 0.8 mL of acetonitrile, but decreased with further increases from 0.8 to 2.0 mL (Fig. 6E). When the volume of elution solvent was <0.8 mL, OPPs were not completely desorbed, which consequently contributed to a lower ER. Theoretically, the larger the volume of eluent, the higher the extraction recovery. However, the volume of eluent is always chosen as a compromise between achieving complete immersion of the nanomaterials and minimizing analyte dilution to reduce the required volume of elution solvent.[32] In this investigation, when the volume of acetonitrile was larger than 0.8 mL, the hybrid nanocomposites were over-immersed. Under such circumstance, due to saturated or excessive adsorption by nanocomposites, the volume of eluent collected after elution would be greatly lost, thus leading to the decrease of extraction

recovery. Thus, an elution solvent volume of 0.8 mL was selected as the optimum volume.

Based on the optimization studies, the selected experimental conditions were: Na_2CO_3 + TTA as tablet acidic and alkaline sources; eluent, 0.8 mL of acetonitrile; composite mass, 15 mg; and extraction/adsorption time, 6 min.

3.3. Comparison of ERs with effervescence and no effervescence (hand-shaking)

To evaluate whether an effervescent reaction is conductive to enhanced dispersive efficiency for the $NiFe_2O_4$@SiO_2@PANI-IL nanocomposites, we compared the ERs for OPPs in the presence or absence of effervescent reaction. Direct addition of nanocomposites with a 4 min hand-shaking yielded ERs for the four OPPs in the range of 79.3 to 85.4% (Fig. 6F). In contrast, use of the effervescent tablets (CO_2 bubbles lasting for $\sim$4 min) increased the average ERs to the range of 88.4 to 93.7%, an absolute increase of $\sim$9.0% as compared to hand-shaking treatments. In particular, ERs for methamidophos and parathion reached as high as 93.7 and 92.8%, respectively, upon effervescent reaction (Fig. 6F). Therefore, we posit that integration of $NiFe_2O_4$@SiO_2@PANI-IL into the effervescent tablet contributed to greater dispersion of the nanocomposites, thereby increasing the ERs for OPPs in the ERMSE method. Moreover, utilization of effervescent tablets avoids the need for an external physical energy source, such as ultrasound or vortexing, making the methodology feasible for remote and outdoor use.

3.4. Comparison of ERs by $NiFe_2O_4$, $NiFe_2O_4$@SiO_2 and $NiFe_2O_4$@SiO_2@PANI-IL

The effects of SiO_2 and PANI-IL coatings on the ERs for OPPs were investigated among the three MNPs ($NiFe_2O_4$, $NiFe_2O_4$@-SiO_2 and $NiFe_2O_4$@SiO_2@PANI-IL) using the aforementioned optimized conditions. When $NiFe_2O_4$ was used as the adsorbent/extractant, the average ER for OPPs was 56.7%, which compared to 75.4 % for the $NiFe_2O_4$@SiO_2 treatment (Fig. S1†). This $\sim$19% increase in ERs can be ascribed to the SiO_2-coated $NiFe_2O_4$ having increased contact area with analytes in the aqueous solution and reduced agglomeration of MNPs, thereby

Table 1 Analytical performance of the ERMSE/HPLC-DAD method in fruit juice samples[a]

Analyte	Liner range ($\mu g\ L^{-1}$)	R^2	LODs ($\mu g\ L^{-1}$)	LOQs ($\mu g\ L^{-1}$)	Intra-day RSDs (%, $n = 6$)			Inter-day RSDs (%, $n = 6$)		
					Low	Medium	High	Low	Medium	High
Methamidophos	0.45–500	0.9963	0.13	0.45	2.3	4.2	3.2	1.1	3.4	4.8
Malathion	0.37–500	0.9987	0.11	0.37	2.4	1.5	4.3	4.4	3.7	5.2
Parathion	0.17–500	0.9991	0.17	0.58	3.3	1.8	3.6	3.2	2.1	4.6
Diazinon	0.21–500	0.9945	0.06	0.21	1.9	3.8	3.5	2.8	4.5	3.6

[a] (1) LRs, linear ranges; R^2, coefficients of determination; LODs, limits of detection at S/N = 3; LOQs, limits of quantitation at S/N = 10; and RSDs, relative standard deviations ($n = 6$). (2) Precision experiments were conducted under the following conditions: (a) OPPs at the three fortification levels in apple juice; (b) $NiFe_2O_4$@SiO_2@PANI-IL nanocomposites as absorbent, 15 mg; acetonitrile as eluent, 0.8 mL; extraction time, 6 min; Na_2CO_3 + TTA, 8 mm diameter × 2.5 mm thickness. (3) "Low, Medium and High" indicates 5, 20 and 200 $\mu g\ L^{-1}$ fortification levels in apple fruit samples, respectively.

improving the adsorption efficiency. In contrast, SiO$_2$@PANI-IL-coated NiFe$_2$O$_4$ nanoparticles yielded average ERs as high as 88.3%, an increase of *ca.* 31% and 13% over those of NiFe$_2$O$_4$ and NiFe$_2$O$_4$@SiO$_2$, respectively. These results demonstrate that the introduction of SiO$_2$, PANI and IL onto the surface of NiFe$_2$O$_4$ nanoparticles prominently enhance adsorption/extraction efficiency for OPPs.

3.5. Validation of the ERMSE/HPLC-DAD method

Under optimized conditions, this proposed method was evaluated in the context of linear range (LR), coefficient of determination (R^2), limits of detection (LODs, based on S/N = 3), limits of quantitation (LOQs, based on S/N = 10), as well as intra- and inter-day precisions. The LRs were 0.21–0.58–500 µg L^{-1} for methamidophos, malathion, parathion and diazinon (Table 1). R^2 values ranged from 0.9945 to 0.9991, and the LODs and LOQs were 0.06–0.17 µg L^{-1} and 0.21–0.58 µg L^{-1} for the four OPPs, respectively. Intra- and inter-day precisions, expressed as relative standard deviations (RSDs), were 1.5–4.3% and 1.1–5.2%, respectively, at three fortification levels (5, 20 and 200 µg L^{-1}; n = 6).

3.6. Real sample analysis

To evaluate real-world applicability, five fruit juice samples (apple, pear, orange, peach, mango) were extracted by the ERMSE method, and subsequently analyzed by HPLC/DAD. Good ERs were obtained for all four OPPs from the fruit juice samples: methamidophos = 81.3–96.5%, malathion = 80.6–95.4%, parathion (83.5–97.1%) and diazinon (81.4–97.3%) (Table 2). Fig. 7 shows typical chromatograms of the four OPPs detected in fruit juices by the ERMSE/HPLC-DAD method. In summary, the newly developed method satisfies the technical
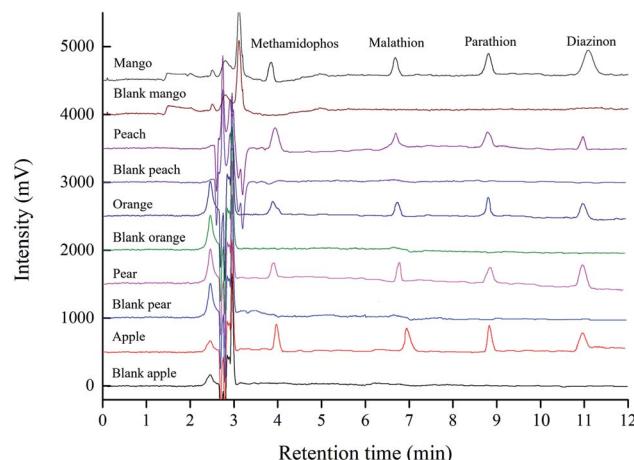

Fig. 7 Typical chromatograms of four OPPs by the ERMSE/HPLC-DAD method. Note: Optimized ERMSE conditions: OPP fortification level of 5 µg L^{-1}; volume of eluent (acetonitrile), 0.8 mL; composite mass, 15 mg; no salt addition and extraction/adsorption time, 6 min.

requirements for trace-level detection of OPPs in complex fruit juice matrices with high precision and accuracy.

3.7. Recycling of the NiFe$_2$O$_4$@SiO$_2$@PANI-IL nanocomposites

MNP reusability (*i.e.*, recycling) is an important metric for improving the application potential of nanocomposites.[33] We analyzed reusability of the NiFe$_2$O$_4$@SiO$_2$@PANI-IL adsorbent by regenerating with three washing cycles of ethanol and water, and subsequent drying for use in another effervescent-tablet preparation and extraction cycle. As a result, the three-layer core–shell nanomaterial could be reused for at least eight cycles with ER losses of <10%, suggesting that the nanocomposites retains excellent recyclability and stability (Fig. S2†).

Table 2 The fortified recoveries for OPPs in fruit juice samples^a

Sample	Methamidophos Added (µg L^{-1})	Found (µg L^{-1})	ER (%)	Malathion Added (µg L^{-1})	Found (µg L^{-1})	ER (%)	Parathion Added (µg L^{-1})	Found (µg L^{-1})	ER (%)	Diazinon Added (µg L^{-1})	Found (µg L^{-1})	ER (%)
Apple juice	5	4.2 ± 0.04	84.3	5	4.8 ± 0.05	95.4	5	4.7 ± 0.02	94.6	5	4.6 ± 0.01	91.1
	20	18.3 ± 0.13	91.3	20	18.6 ± 0.04	93.2	20	19.4 ± 0.17	97.1	20	17.5 ± 0.14	87.4
	200	191.2 ± 0.05	95.6	200	172.2 ± 0.28	86.1	200	173.2 ± 0.21	86.6	200	192.4 ± 0.37	96.2
Pear juice	5	4.5 ± 0.06	90.2	5	4.4 ± 0.10	88.3	5	4.4 ± 0.03	87.1	5	4.3 ± 0.02	87.3
	20	16.3 ± 0.21	81.3	20	18.2 ± 0.21	91.7	20	16.7 ± 0.24	83.5	20	16.5 ± 0.33	82.6
	200	177.2 ± 0.34	88.6	200	161.8 ± 0.35	80.9	200	182.0 ± 0.22	91.0	200	162.8 ± 0.24	81.4
Orange juice	5	4.8 ± 0.01	96.5	5	4.7 ± 0.02	93.6	5	4.4 ± 0.04	88.6	5	4.7 ± 0.02	93.5
	20	18.9 ± 0.54	94.3	20	16.1 ± 0.25	80.6	20	18.7 ± 0.13	93.4	20	18.9 ± 0.21	94.8
	200	166.2 ± 0.24	83.1	200	175.0 ± 0.13	87.5	200	179.4 ± 0.28	89.7	200	191.0 ± 0.30	95.5
Peach juice	5	4.2 ± 0.08	84.3	5	4.6 ± 0.01	91.6	5	4.3 ± 0.02	85.3	5	4.9 ± 0.01	97.3
	20	16.6 ± 0.15	82.9	20	17.7 ± 0.22	88.4	20	19.4 ± 0.08	96.8	20	17.5 ± 0.17	87.3
	200	178.2 ± 0.22	89.1	200	163.8 ± 0.18	81.9	200	170.6 ± 0.15	85.3	200	169.8 ± 0.41	84.9
Mango juice	5	4.7 ± 0.11	93.7	5	4.2 ± 0.04	83.4	5	4.2 ± 0.03	84.5	5	4.5 ± 0.03	90.4
	20	17.1 ± 0.23	85.5	20	18.7 ± 0.36	93.7	20	18.7 ± 0.19	93.6	20	17.8 ± 0.26	89.1
	200	181.2 ± 0.37	90.6	200	171.6 ± 0.21	85.8	200	188.4 ± 0.28	94.2	200	167.2 ± 0.33	83.6

^{a} (1) ER indicates extraction recovery; (2) each treatment includes three replicates (n = 3); (3) each detected value is mean ± SD (standard deviation, n = 3); (4) experimental conditions: NiFe$_2$O$_4$@SiO$_2$@PANI-IL as absorbent, 15 mg; 0.8 mL of acetonitrile as eluent; extraction time, 6 min.

Table 3 Comparison of the ERMSE/HPLC-DAD method with previously reported methods for the determination of OPPs in fruit juices[a]

Pretreatment method	Type of nanomaterial as adsorbent	RSD (%)	LOD ($\mu g\ L^{-1}$)	Extraction time (min)	ERs (%)	References
MSPE/HPLC-DAD	MOFs, MIL-101	1.1–7.8	0.3–1.5	20	80.2–107.5	7
MSPE/HPLC-UV	Fe_3O_4/C	2.7–7.6	4.3–47.4	5	79.6–103.5	36
MSPE/HPLC-UV	MHMS-MCNPs	<4.6	0.07	3	74–104.8	29
MSPE/HPLC-UV	Fe_3O_4@SiO_2@KIT-6	0.1–5.5	0.005–0.01	10	86.6–98.8	8
MSPE/HPLC-UV	PIL-MNPs	4.5–11.3	0.01	2	81.4–112.6	34
ETMSE/HPLC-DAD	$NiFe_2O_4$@SiO_2@PANI-IL	1.1–5.2	0.06–0.17	6	80.6–97.3	This work

[a] (1) MOFs, metal organic frameworks; (2) Fe_3O_4/C, carbon coated Fe_3O_4; (3) MHMS-MCNPs, mixed hemimicelle SDS-coated magnetic chitosan nanoparticles; (4) Fe_3O_4@SiO_2@KIT-6, mesoporous KIT-6-magnetite composite; (5) PIL-MNPs, poly (ionic liquid) immobilized magnetic nanoparticles; (6) MSPE-HPLC-UV, magnetic solid-phase extraction combined with high-performance liquid chromatography-ultraviolet detection; (7) MSPE-HPLC-DAD, magnetic solid-phase extraction combined with high-performance liquid chromatography-diode array detection.

Thus, the $NiFe_2O_4$@SiO_2@PANI-IL nanomaterial possesses excellent characteristics for long-term use in the monitoring of trace OPPs in fruit juice samples.

3.8. Comparison of the ERMSE/HPLC-DAD method with previously reported methods

A comparison of the present method with previously reported methods for the determination of OPPs was conducted in the context of type of adsorbent, RSD, LODs, extraction time and ERs (Table 3).[4,5,28,29,34] The ERMSE/HPLC-DAD method has the following advantages: (1) it is fast with the whole adsorption/extraction process completed within 6 min. Effervescent tablet-assisted diffusion provides rapid and effective dispersion of the nanocomposites. The adsorption/extraction time (6 min) for the new method is prominently lower than those of MOFs-based MSPE (20 min)[4] and Fe_3O_4@SiO_2@KIT-6-based MSPE (10 min);[5] (2) it possesses higher sensitivity for OPPs with LODs of 0.06–0.17 $\mu g\ L^{-1}$ and higher repeatability with intra- and inter-day precisions of 1.1–5.2% as compared to those of MIL-101-based MSPE-HPLC-DAD (LODs of 0.3–1.5 $\mu g\ L^{-1}$)[4] and Fe_3O_4/C-based MSPE-HPLC-UV (LODs of 4.3–47.4 $\mu g\ L^{-1}$).[28] It provides comparable LODs with those of MHMS-MCNPs-based MSPE/HPLC-UV (0.07 $\mu g\ L^{-1}$)[29] and PIL-MNPs-based MSPE/HPLC-UV (0.01 $\mu g\ L^{-1}$);[34] (3) it avoids the utilization of traditional organic dispersive solvents (methanol, acetonitrile, acetone, *etc.*) in conventional microextraction procedures; (4) the utilization of a "green" solvent in the nanocomposites and recyclable MNCs make the method more environment friendly. Overall, the $NiFe_2O_4$@SiO_2-PANI-IL-based ERMSE/HPLC-DAD method is simple, rapid, easy to use and benign to the environment, and thus shows great prospective for routine trace monitoring of OPP residues in complex fruit juice matrices.

3.9. Recycling of the $NiFe_2O_4$@SiO_2@PANI-IL nanocomposites

MNP reusability (*i.e.*, recycling) is an important metric for improving the application potential of nanocomposites.[33] We analyzed reusability of the $NiFe_2O_4$@SiO_2@PANI-IL adsorbent by regenerating with three washing cycles of ethanol and water, and subsequent drying for use in another effervescent-tablet preparation and extraction cycle. As a result, the three-layer core–shell nanomaterial could be reused for at least eight

cycles with ER losses of <10%, suggesting that the nano-composites retains excellent recyclability and stability (Fig. S2†). Thus, the $NiFe_2O_4$@SiO_2@PANI-IL nanomaterial possesses excellent characteristics for long-term use in the monitoring of trace OPPs in fruit juice samples.

4. Conclusions

An ERMSE method, based on utilization of effervescent tablets and $NiFe_2O_4$@SiO_2@PANI-IL nancomposites, was developed for the enhanced extraction of OPPs in fruit juices prior to HPLC-DAD detection. Vigorous CO_2 effervescent bubbles contributed to homogeneous dispersion of nanocomposites, which enhanced interactions between OPPs and the nano-sorbents. The superparamagnetism of nanocomposites was conductive to rapid separation/collection of the adsorbent from the aqueous phase. Moreover, the attachment of SiO_2, PANI and ILs onto the surface of $NiFe_2O_4$ enhanced active sites, pore size/volume and stability, thereby enhancing extraction capacity. Under optimized conditions, the ERMSE method gave high precision with RSDs of 1.1–5.2%, low LODs of 0.06–0.17 $\mu g\ L^{-1}$ and satisfactory recoveries of 80.6–97.3% in apple, pear, orange, peach and mango fruit juices. Notably, the $NiFe_2O_4$@SiO_2@PANI-IL nancomposites can be recycled at least eight times with ER losses <10%. Consequently, the newly developed method provides a simple, efficient, and green method requiring no dispersive solvents or auxiliary devices, thereby providing wide application value in conventional monitoring of OPPs in fruit juice matrices and potential other food/environmental matrices.

Conflicts of interest

There are no conflicts of interest to declare.

Acknowledgements

References

1 D. Li, M. He, B. Chen and B. Hu, *J. Chromatogr. A*, 2019, **1583**, 19.

2 H. Heidaria, S. Ghanbari-Rada and E. Habibib, *Journal of Food Composition and Analysis*, 2020, **87**, 103389.

3 L. Du, X. Wang, T. Liu, J. Li, J. Wang, M. Gao and H. Wang, *Microchem. J.*, 2019, **150**, 104128.

4 L. Gao, L. Liu, Y. Sun, W. Zhao and L. He, *Microchem. J.*, 2020, **153**, 104364.

5 A. Lago, M. Cavalcanti, M. Rosa, A. Silveira, C. Tarley and E. Figueiredo, *Anal. Chim. Acta*, 2020, **1102**, 11.

6 D. Garcia-Rodriguez, R. Cela-Torrijos, R. A. Lorenzo-Ferreira and A. M. Carro-Diaz, *Food Chem.*, 2012, **135**, 259.

7 H. Zhao, Y. Dong, G. Wang, P. Jiang, J. Zhang, L. Wu and K. Li, *Chem. Eng. J.*, 2013, **219**, 295.

8 M. Ait Tamerd, B. Abraime, A. Lahmar, M. E. Marssi, M. Hamedoun, A. Benyoussef and A. E. Kenz, *Superlattices Microstruct.*, 2020, **139**, 106401.

9 H. Zhang, B. Xia, P. Wang, Y. Wang, Z. Li, Y. Wang, L. Feng, X. Li and S. Du, *J. Alloys Compd.*, 2020, **819**, 153053.

10 Z. Lia, Y. Liu, S. Zoub, C. Lu, H. Bai, H. Mu and J. Duan, *Chem. Eng. J.*, 2020, **382**, 123008.

11 G. Su, Q. Zheng, Y. Wang, J. Liu and J. Xiang, *J. Nanosci. Nanotechnol.*, 2018, **18**, 2665.

12 G. Jimenez-Skrzypek, J. G. Salamo, D. A. Varela-Martinez, M. A. Gonzalez-Curbelo and J. Hernandez-Borges, *J. Chromatogr. A*, 2020, **1611**, 460620.

13 C. Hu, M. He, B. Chen and B. Hu, *J. Chromatogr. A*, 2015, **1394**, 36.

14 M. S. Shahriman, M. R. Ramachandran, N. N. M. Zain, S. Mohamad, N. S. A. Manan and S. M. Yaman, *Talanta*, 2018, **178**, 211.

15 F. V. A. Dutra, B. C. Pires, M. M. Coelho, R. A. Costa, C. S. Francisco, V. L. Junior and K. B. Borges, *Microchem. J.*, 2020, **153**, 104490.

16 X. Yang, K. Qiao, F. Liu, X. Wu, M. Yang, J. Li, H. Gao, S. Zhang, W. Zhou and R. Lu, *Talanta*, 2017, **166**, 93.

17 M. He, S. Su, B. Chen and B. Hu, *Talanta*, 2020, **207**, 120314.

18 J. Wang, W. Zhu, T. Zhang, L. Zhang, T. Du, W. Zhang, D. Zhang, J. Sun, T. Yue, Y. Wang and J. Wang, *Anal. Chim. Acta*, 2020, **1100**, 57.

19 P. Li, Y. Lu, J. Cao, M. Li, C. Yang and H. Yan, *J. Chromatogr. A*, 2020, **1623**, 461192.

20 P. Zhou, K. Chen, M. Gao, J. Qu, Z. Zhang, R. A. Dahlgren, Y. Li, W. Liu, H. Huang and X. Wang, *Food Chem.*, 2018, **268**, 468.

21 L. Li, M. Wu, Y. Feng, F. Zhao and B. Zeng, *Anal. Chim. Acta*, 2016, **948**, 48.

22 X. L. Yang, K. X. Qiao, F. Liu, X. L. Wu, M. Y. Yang, J. Li, H. X. Gao, S. B. Zhang, W. F. Zhou and R. H. Lu, *Talanta*, 2017, **166**, 93.

23 Y. Li, J. Hu, W. Liu, L. Jin, P. Zhou, Y. Zhang, B. Zhang, Z. R. A. Dahlgren, X. Wang and Y. Zhou, *Talanta*, 2019, **195**, 785.

24 P. Zhou, R. Zheng, W. Zhang, W. Liu, Y. Li, H. Wang and X. Wang, *J. Anal. At. Spectrom.*, 2019, **34**, 598.

25 S. Wang, X. Pang, J. Cao, W. Cao, J. Xu, Q. Zhu, Q. Zhang and L. Peng, *J. Chromatogr. A*, 2015, **1418**, 12.

26 H. Kavas, A. Baykal, M. S. Toprakc, Y. Köseoglu, M. Sertkol and B. Aktas, *J. Alloys Compd.*, 2009, **479**, 49.

27 N. H. Nasab and J. Safari, *J. Mol. Struct.*, 2019, **1193**, 118.

28 X. Sun, Y. Q. Ma, S. T. Xu, Y. F. Xu and B. G. Geng, *Mater. Charact.*, 2015, **107**, 343.

29 M. George, A. K. Pandey, N. A. Rahim, V. V. Tyagi, S. Shahabuddin and R. Saidur, *Sol. Energy*, 2020, **204**, 448.

30 W. Ding, X. Wang, T. Liu, M. Gao, F. Qian, H. Gu and Z. Zhang, *Microchem. J.*, 2019, **150**, 104109.

31 J. Wu, J. Li, Y. Chen, X. Bao, H. Tang, S. Ma, S. Zhou, M. Xu, J. Tao, W. Wang and X. Wang, *Food Analytical Methods*, 2019, **12**, 2106.

32 W. Ding, X. D. Wang, T. T. Liu, H. D. Gu and Z. N. Zhang, *Microchem. J.*, 2019, **150**, 104109.

33 C. Tan, J. Li, W. Liu, Q. Zhao, X. Wang and Y. Li, *Chem. Eng. J.*, 2020, **396**, 125191.

34 S. R. Bandforuzi and M. R. Hadjmohammadi, *Anal. Chim. Acta*, 2018, **1078**, 90.